Hubble Space Telescope Observations of the CfA Seyfert 2s: Near-infrared Surface Photometry and Nuclear Bars[1]

Paul Martini [2], Richard W. Pogge[3], Swara Ravindranath[2,4], Jin H. An[3]

ABSTRACT

We present near-infrared (NIR) J and H surface photometry of 24 of the nearby Seyfert 1.8, 1.9 and 2 galaxies from the CfA Seyfert sample. The excellent angular resolution of the *Hubble Space Telescope* (*HST*) probes spatial scales as small as tens of parsecs in most of these AGN and is sensitive to the presence of nuclear bars and other potential signatures of the AGN fueling process that channels host galaxy gas and dust to the nuclear region. We have used elliptical isophote techniques to search for nuclear bars in all of these galaxies and have employed a two-dimensional fitting technique to model the nuclear point source and surface brightness distribution of a bright subsample of these galaxies in an attempt to alleviate the impact of the nuclear point source on our sensitivity to nuclear bars. We find stellar nuclear bar candidates in four of these galaxies: Mrk 471, Mrk 270, Mrk 573, and NGC 5929, nearly 20% of the total sample. The percentage rises to $\sim$ 30% when systems with disturbed morphologies or high inclinations are excluded. The nuclear bars in Mrk 573 and Mrk 270 exhibit some evidence for dust lanes along their leading edges, analogous to the structures seen in host galaxy bars, while the dust lanes in Mrk 471 and NGC 5929 exhibit a more complex morphology. The fact that most of these AGN do not appear to contain stellar nuclear bars suggests that they are not the fueling mechanism for most low-luminosity AGN.

Subject headings: galaxies: active – galaxies: photometry – galaxies: Seyfert – galaxies: structure – infrared: galaxies

---

[1]Based on observations with the NASA/ESA *Hubble Space Telescope* obtained at the the Space Telescope Science Institute, which is operated by the Association of Universities for Research in Astronomy, Incorporated, under NASA contract NAS5-26555.

[2]Carnegie Observatories, 813 Santa Barbara St., Pasadena, CA 91101-1292, martini@ociw.edu, swara@ociw.edu

[3]Department of Astronomy, Ohio State University, 140 W. 18th Ave., Columbus, OH 43210, pogge@astronomy.ohio-state.edu, jinhan@astronomy.ohio-state.edu

[4]Department of Astronomy, University of California, Berkeley, CA 94720-3411

1. Introduction

Bars and mergers have been the most commonly proposed fueling mechanisms for low-luminosity active galactic nuclei (AGN). While both of these methods can remove angular momentum from gas and dust, neither of these processes have been proven to be the sole arbiter of the AGN fueling process. Large-scale bars occur with equal frequency in normal and active galaxies (McLeod & Rieke 1995; Mulchaey & Regan 1997; Ho et al. 1997a, though see Knapen et al. 2000) and most low-luminosity AGN do not show any evidence of a recent major merger event (Fuentes-Williams & Stocke 1988). Recent, careful searches for evidence of minor mergers have also not found a clear excess of faint companions around these AGN (De Robertis et al. 1998).

This lack of success in finding a definitive fueling mechanism for all low-luminosity AGN has driven observers to search at ever higher spatial resolution for signatures of the mechanisms that could remove sufficient angular momentum from gas and dust within the central few hundred parsecs. One small-scale feature that could fuel AGN activity (Shlosman et al. 1989; Pfenniger & Norman 1990) is a nuclear bar, which were first observed in nearby, large galaxies as enhancements in the surface brightness distribution (de Vaucouleurs 1975; Kormendy 1979; Buta 1986a,b). The nuclear bars first proposed to fuel AGN activity by Shlosman et al. (1989) were purely gaseous nuclear bars. In their model a large-scale bar leads to the transport of gas into the central region of the galaxy where it forms a circumnuclear gaseous disk. This disk could then become unstable to the formation of a purely gaseous, nuclear bar nested inside the larger bar and this gaseous nuclear bar could drive sufficient material inwards to fuel an AGN. Potentially the best method to detect gaseous nuclear bars is to observe their dust content in absorption against the background stellar light of the far side of the host galaxy. Gaseous nuclear bars may take the form of a bar-shaped dust lane and recently Maiolino et al. (2000) found a straight, or bar-shaped dust lane in Circinus (a Seyfert 2), where the gas kinematics were consistent with this interpretation.

Most of the nuclear bars observed to date have been stellar, rather than gaseous, nuclear bars as they correspond to clear enhancements in the visible or NIR surface brightness distribution. Stellar nuclear bars could also fuel AGN activity by removing angular momentum from circumnuclear material on small scales (Pfenniger & Norman 1990; Friedli & Martinet 1993). As stellar nuclear bars appear to be randomly oriented with respect to host galaxy bars (Buta & Crocker 1993), fairly complex orbits are required to enhance the stellar density and create a stellar nuclear bar composed of old stars (Pfenniger & Norman 1990; Maciejewski & Sparke 1997; Erwin & Sparke 1999a; Maciejewski & Sparke 2000). Stellar nuclear bars selected by their enhancement of the surface density have been found in several AGN hosts, including NGC 2681 and NGC 3945 (Erwin & Sparke 1999a). A recent, kinematic study of

four nuclear bar candidates selected on the basis of NIR surface brightness by Emsellem et al. (2001) found that the velocity fields of three of these galaxies were well-fit by a bar model. The fourth galaxy with a nuclear bar candidate instead hosts a kinematically decoupled gaseous disk and spiral structure within the inner Linblad resonance.

Stellar nuclear bars could also form straight dust lanes similar to those observed in many strongly barred galaxies (e.g. NGC 7479 & NGC 1530, Quillen et al. 1995; Regan et al. 1997). A strong triaxial potential can lead to significant gas inflow in large-scale bars (Athanassoula 1992) and if similar gas flow occurs in nuclear stellar bars, they may have associated dust lanes. Regan & Mulchaey (1999) argued that stellar nuclear bars could be more readily detected by searching for their influence on the ISM as the stellar surface density contrast may be quite weak due to the high velocity dispersion in galactic bulges. They searched for such straight dust lanes in color maps of 12 Seyfert galaxies constructed from visible and NIR *HST* images and found straight dust lanes extending into the nuclear region in NGC 3081, NGC 5347, and NGC 7743. Martini & Pogge (1999) performed a similar search with $V-H$ and $J-H$ *HST* color maps and found straight dust lanes in Mrk 573, Mrk 270, and Mrk 471 in the sample of 24 Seyfert 2s we describe in this paper. Recently, Maciejewski et al. (2001) have argued that in dynamically stable configurations the nuclear bar does not extend to its corotation radius and thus it will not form the strong shocks and corresponding dust lanes seen in large-scale bars sought by Regan & Mulchaey (1999) and Martini & Pogge (1999).

Both of these studies of relatively large numbers of AGN concluded that stellar nuclear bars were present in only a minority of AGN based on selection by the presence of straight dust lanes, rather than enhancements in the stellar surface density. Martini & Pogge (1999) also searched by visual inspection for stellar nuclear bars in the NIR surface brightness contours and found most of the galaxies with straight dust lanes also showed evidence for nuclear bars in the stellar distribution, yet they did not employ a quantitative set of selection criteria. In addition, the results of Maciejewski et al. (2001) suggest that many nuclear bars would be missed in selection based on the presence of straight dust lanes. For the remainder of this paper we will concentrate on stellar nuclear bars selected by their associated starlight and refer to them as simply nuclear bars; we will explicity refer to stellar nuclear bars selected by dust morphology or purely gaseous nuclear bars when appropriate. Nuclear bars are also commonly referred to as secondary bars when they are found in galaxies with large-scale bars, although we will not use this terminology as our sample was not previously selected to only contain galaxies with large-scale bars.

The recent visible and near-infrared (NIR) studies of the circumnuclear regions of low-luminosity AGN with *HST* described above also found that most contain dusty "nuclear" spiral structure on 100s of parsec scales that is distinct from the main disk spiral arms.

These studies found that many AGN have dusty nuclear spiral structure (Quillen et al. 1999; Regan & Mulchaey 1999; Martini & Pogge 1999). Similar nuclear spiral structure has also been observed in a number of quiescent galaxies (Phillips et al. 1996; Carollo et al. 1998; Elmegreen et al. 1998; Laine et al. 1999). Martini & Pogge (1999) estimated that the gaseous disks were not self-gravitating based on a measure of the total extinction in the nuclear spiral arms. They concluded that these spiral structures could be due to shocks propagating in circumnuclear gaseous disks, a mechanism proposed by Elmegreen et al. (1998) and Montenegro et al. (1999). Such shocks could dissipate sufficient angular momentum to fuel these low-luminosity AGN, which only require mass accretion rates of $\sim 0.01 - 0.1 M_{\odot}$ yr^{-1}. Nuclear spiral structure is a tempting signature of the AGN fueling process because, unlike nuclear bars and interactions, it appears to be present in all AGN that do not have morphologically disturbed circumnuclear regions. While there has not yet been a systematic control study to assess the relative frequency of nuclear spiral structure in a control sample of quiescent galaxies, recent *HST* studies of nearby spirals have not found that nuclear spiral structure is similarly ubiquitous in normal galaxies (e.g. Carollo et al. 1998).

In this paper we present a detailed study of the NIR surface photometry from Martini & Pogge (1999), which include 24 of the 25 Seyferts classified as type 1.8, 1.9, or 2 by Osterbrock & Martel (1993) from the CfA Redshift Survey (Huchra & Burg 1992) and listed in Table 1. The main goal of the present paper is to reanalyze the nuclear bar fraction in this sample using a quantitative bar detection algorithm based on the NIR surface brightness distribution in order to test the hypothesis that nuclear bars are responsible for fueling all low-luminosity AGN activity. Given the recent theoretical investigation of Maciejewski et al. (2001), dynamically stable nuclear bars may not form the straight dust lanes used to select previous nuclear bar samples and therefore nuclear bars selected by the NIR surface brightness distribution may provide a stronger constraint on the importance of nuclear bars to the AGN fueling process. In addition to our search for nuclear bars, we also measure the surface brightness profiles for all of these galaxies and derive the best-fit profile parameters and nuclear luminosities for a subset of galaxies that are sufficiently bright and not in edge-on or morphologically disturbed systems.

2. Image Processing

These images were all obtained with the NICMOS Camera 1 (NIC1) on *HST* , which has a plate scale of $0.043''$ pixel^{-1}. With the exception of NGC 1068 (Thompson & Corbin 1999), all of these galaxies were observed as part of GO-7867. We observed them through

the F110W and F160W filters for 1024s per filter, split into four dither positions (SPIRAL-DITH) of 256s and offset one arcsecond to aid bad pixel rejection. The F110W and F160W filters (F110M and F170M for NGC 1068) are roughly equivalent to the ground-based J and H filters, respectively.

The images were processed through the standard CALNICA data reduction pipeline from STScI. As noted by Martini & Pogge (1999), we did not use the CALNICB part of the STScI pipeline to combine our four dithered images. CALNICB attempts to subtract the sky level from an image sequence when it shifts and adds the individual dither positions. In our images, however, even the faintest objects fill nearly half of the field, and so a sky subtraction is impossible. In any event, the sky background for these images through the J and H filters is negligible based on measurements of both the more compact galaxies in our sample and archival, blank fields with the same instrument configuration. Instead of CALNICB, we used simple integer shifts to align and stack the four dither positions.

The photometric calibration of *HST* data is in general nontrivial due to differences between *HST* filters and their nearest ground-based analogs. The F110W and F160W filters in NICMOS are broader than the standard, ground-based J and H filters and include spectral regions in these galaxies that are unobservable from the ground due to telluric water absorption. To transform our images to the ground-based CTIO/CIT photometric system (Elias et al. 1982; Persson et al. 1998), we used the photometric zeropoints established by the NICMOS photometric calibration program and the color terms calculated by Stephens et al. (2000). Stephens et al. (2000) calculated a complete photometric solution for NICMOS Camera 2 (NIC2) based on observations of red standards, in addition to the bluer standards observed as part of the NICMOS photometric calibration program. To calibrate our NIC1 data, we used the STScI zeropoint calibration and supplemented it with the color terms from Stephens et al. (2000). While these color terms were derived for a different camera, they should be dominated by the wavelength dependence of the filter transformation and array quantum efficiency and these quantities are nearly identical for NIC1 and NIC2. For NGC 1068 we used the standard NICMOS photometric calibration.

3. Surface Photometry and Nuclear Bars

Figures 1 – 4 show J and H images (*top panels*) for this sample. These grayscale images show the wealth of different morphologies present in the central regions of Seyferts. One qualitative trend is the strength of the nuclear point source with Seyfert type. The Seyfert 2 galaxies have on average weaker nuclear point sources than the 1.9s and 1.8s. This agrees with the trend observed in previous visible-wavelength *HST* observations of

Seyferts, where Seyfert 1s tend to have extremely bright nuclear sources and Seyfert 2s have a significantly weaker nuclear contribution (Nelson et al. 1996; Malkan et al. 1998). Two interesting exceptions are the extremely strong nuclear point sources in the Seyfert 2s NGC 1068 and NGC 7674 (Figures 3 and 4), which harbor polarized broad line regions (Miller & Antonucci 1983; Miller & Goodrich 1990). To a lesser extent Mrk 573 and NGC 5347 (Figures 3 and 4) appear to have stronger nuclear point sources than the other Seyfert 2s.

We used the ELLIPSE task in IRAF[5] STSDAS to fit elliptical isophotes to these galaxies and measure the surface brightness, ellipticity ($\epsilon = 1 - b/a$), and position angle of the semimajor axis (PA, in degrees measured north through east). ELLIPSE fits elliptical isophotes according to the formalism outlined by Jedrzejewski (1987) and includes measurement of higher order Fourier coefficients that characterize the deviation of the isophotes from perfect ellipses. The lower panels in Figure 1 – 4 (*top to bottom*) show the J and H surface brightness profile, ellipticity, and position angle as a function of semimajor axis. The quality of the flat field and instrumental background subtraction can affect the elliptical isophotes on large scales. The nuclei of nearly all of these galaxies fall on one of the lower two quadrants of the NIC1 array, which have higher quantum efficiency than the upper-left quadrant. The low quantum efficiency of the upper-left quadrant requires a large flatfield correction and uncertainties in the bias level and the flatfield could systematically distort the elliptical isophote fits. In order to verify that we were not affected by this systematic source of error, we constructed a data quality file for the ELLIPSE package that masked out the lowest quantum efficiency regions in the upper-left quadrant of the NIC1 array. We also visually inspected the ellipse fits to each galaxy to insure that the position angle at large semimajor axis was not artificially twisted by any errors in the flatfield.

On smaller angular scales, the structure in the NICMOS point spread function (PSF) can significantly affect the quality of the fits to some of these galaxies. This is particularly striking in the Seyfert 1.8 galaxies (e.g. Mrk 334 or UGC 12138, Figure 1) where the "bump" clearly visible in the surface brightness profile is due to the first Airy ring of the PSF at $r_J \sim 0.15''$ and $r_H \sim 0.23''$. The ellipse fits for strong nuclear point sources also tend to include a strong fourth-order Fourier coefficient due to the nonaxisymmetric, "boxy" diffraction pattern in the PSF. These cause the ellipticity and position angle distributions to have large errors and scatter until the influence of the first Airy ring falls off at $\sim 0.3''$, or even until higher order diffraction patterns diminish at $\sim 0.7''$, such as in Mrk 334, UGC 12138, or NGC 1068. For galaxies with little or no nuclear contribution, the ellipticity and position

[5]IRAF is distributed by the National Optical Astronomy Observatories, which are operated by the Association of Universities for Research in Astronomy, Inc., under cooperative agreement with the National Science Foundation.

angle distributions are reliable for $r_J \geq 0.15''$ and $r_H \geq 0.23''$. The vertical, dashed lines in Figures 1 – 4 correspond to these lower limits in the sensitivity of the measured ellipticity and position angle distributions to nuclear bar candidates.

To quantify the sensitivity of our NIR surface photometry to the presence of nuclear bars, we adopt the criteria used by Mulchaey et al. (1997) to identify host galaxy bars: an increase in ellipticity at constant position angle followed by a drop in ellipticity to the inclination of the disk. As the 11″x11″ NIC1 FOV does not always include much of the host galaxy disk, the final position angle and ellipticity may reflect the presence of a host galaxy bar; we therefore relax the latter criterion. By examination of the ellipticity and position angle profiles in the figures, we find nuclear bar candidates in Mrk 471, Mrk 573, Mrk 270, and NGC 5929. Figure 5 shows the color maps from Martini & Pogge (1999) along with the $H-$band surface brightness contours for these four galaxies. All of these galaxies were suggested to have nuclear bars by Martini & Pogge (1999) based on the appearance of the nuclear surface brightness isophotes, and all but NGC 5929 exhibit straight dust lanes in their visible-NIR color maps. NGC 5347, which was suggested by Regan & Mulchaey (1999) to have the straight dust lanes indicative of a nuclear bar, does not show strong evidence of a nuclear bar in the NIR surface brightness distribution. The lack of NIR morphological evidence precludes the presence of a significant old stellar population associated with a nuclear bar. However, as demonstrated by Regan & Mulchaey (1999), a small contrast in the stellar density may excite an order of magnitude larger contrast in the ISM.

Knapen et al. (2000) define a galaxy as barred if the ellipticity varies by $\epsilon \geq 0.1$ over a region of constant position angle or if the position angle changes by $\geq 75^\circ$ over a range where the ellipticity is greater than 0.1. All four of the galaxies classified as barred according to the Mulchaey et al. (1997) classification scheme would also be barred under these similar criteria. Mrk 573 and Mrk 270 meet the first set of criteria as they change in ellipticity at constant position angle, while the remaining two galaxies have changes in position angle corresponding to their ellipticity variations.

The properties of the nuclear bar candidates are summarized in Table 2 and a description of the results for individual galaxies are given in the Appendix. Both Mrk 573 and Mrk 471 have prominent, large-scale bars and therefore could also be termed secondary bars. The remaining two nuclear bars candidates, Mrk 270 and NGC 5929, do not have known large-scale bars. Given their small-scale, they are clearly nuclear bars, but they are not also secondary bars. Mrk 270 was one of the few CfA Seyferts not observed by McLeod & Rieke (1995) in their $K-$band survey, and it is only typed as "SO?" in the RC3 catalog. NGC 5929 is classified as unbarred in the RC3 and by McLeod & Rieke (1995). However, this galaxy is in the midst of an interaction which could have obscured or destroyed the large-scale bar.

Another possibility is that the interaction may have sufficiently disturbed the small-scale morphology to artificially produce the nuclear bar candidate in the NIR isophotes.

As discussed above, the complex NICMOS PSF can introduce significant scatter into the ellipticity and position angle distributions used to identify nuclear bar candidates. Our sensitivity to candidates of a given physical length is therefore sensitive to the distance of a galaxy and the strength of its nuclear point source. This issue is discussed in section 5. For galaxies with sufficient signal-to-noise we have constructed two-dimensional models of the galaxy surface brightness distribution and nuclear point source in an attempt to improve our sensitivity to nuclear bars and parameterize the central light distribution of these Seyferts. This technique is described in the next section.

4. Analysis

The high angular resolution of *HST* that has made it possible to systematically search for nuclear bars and spiral structure in nearby AGN has also revolutionized the study of the central stellar light distribution in galaxies (e.g. Lauer et al. 1995; Faber et al. 1997). Nearly all early-type galaxies with dust in their central regions have compact nuclear sources (Lauer et al. 1995; van Dokkum & Franx 1995; Rest et al. 2001; Ravindranath et al. 2001). While all later-type galaxies usually have significant dust in their nuclear regions, irrespective of whether or not they host an AGN or nuclear star formation, Carollo & Stiavelli (1998) suggested that compact nuclear sources are more common in galaxies with exponential rather than $R^{1/4}$ bulges and that exponential bulges likely have lower stellar densities. Márquez et al. (1999) explored the circumnuclear properties of isolated spirals with and without AGN based on ground-based NIR observations and found no differences in the profile shapes of their AGN host and normal galaxy samples, although they did find that the central colors of AGN are redder than normal spirals (Márquez et al. 2000).

A two-dimensional analysis of the surface brightness distribution was performed in order to quantify the contributions from the galaxy bulge and the nuclear point source. The 2-D decomposition of the components was done using the least–squares fitting program GALFIT (Peng et al. 2001), which models the galaxy light with a combination of various analytic functions (e.g. Sérsic, de Vaucouleurs, Nuker, exponential, Gaussian, Moffat). GALFIT can also simultaneously fit an additional point source (AGN or compact star cluster) and provide a good measurement of the nuclear magnitude.

One of the main concerns while trying to obtain information at the highest spatial resolution is to account for the effects of the PSF. Our images do not have the high signal-to-

noise ratios required for using deconvolution techniques. Instead, the 2-D modeling routine used here convolves the galaxy model with high-quality synthetic PSFs produced by the TINYTIM software (Krist & Hook 1999). The TINYTIM PSFs are adequate for these applications even though there may be uncertainties due to temporal variations like thermal changes in the instrument and shifts in the pupil mask alignment (Krist & Hook 1997).

We fit the galaxy bulge using either a "Nuker" law (Lauer et al. 1995), which has the form:

$$I(r) = 2^{(\beta-\gamma)/\alpha} I_b \left(\frac{r}{r_b}\right)^{-\gamma} \left[1 + \left(\frac{r}{r_b}\right)^{\alpha}\right]^{(\gamma-\beta)/\alpha}, \quad (1)$$

or a Sérsic profile (Sérsic 1968) of the form:

$$I(r) = I_e \exp\left(-b\left[\left(\frac{r}{r_s}\right)^{1/n} - 1\right]\right) \quad (2)$$

and the nucleus was modeled with a Gaussian function. The details of the fitting procedure are described by Ravindranath et al. (2001).

A major difficulty in trying to decouple the galaxy contribution from the point source arises from the relatively small field of view of the NIC1 images. In a few cases the nucleus is very bright and the diffraction rings are prominent out to 1″ semi-major axis, leaving only a small region for sampling the contribution from the galaxy (e.g., NGC 5674 and NGC 7674, see Figures 2 and 4). We could obtain reasonably good 2-D fits for eleven galaxies in the sample. In most cases, we were able to parametrize the surface brightness using a Nuker function, although for two galaxies we were only able to fit Sérsic profile as it has fewer parameters. The inner slope (γ) values for all the galaxies fall in the range 0.45-0.7 and imply steeper central surface brightness profiles than seen in many earlier-type galaxies (Ravindranath et al. 2001).

The nuclear apparent magnitudes of these AGN are a measure of the luminosity of the accretion onto the central black hole. Combined with observations at other wavelengths, these measurements probe the spectral energy distribution for the accretion process (e.g. Ho 1999). The apparent brightness of many of these nuclear point sources were previously measured by Quillen et al. (2001) and the measurements are in good agreement within the uncertainties. The best-fit galaxy profile parameters along with the apparent magnitude for the nuclear point source are given in Table 3.

The 2-D models are generated for a fixed ellipticity and position angle determined from the isophotal contours in the outer region. Therefore the residual image formed from the difference of the galaxy and model fit enables us to identify features (e.g. dust lanes and bars) that cause significant changes in the ellipticity and position angle. Since the 2-D analysis

includes a fit to the nuclear point source as an additional component, the fit residuals provide a more sensitive probe of underlying nuclear bars at small semi-major axis length in galaxies with a bright nucleus than the simple elliptical isophote fits discussed in section 3. The nuclear bars in Mrk 270, Mrk 573 and NGC 5929 are clearly visible in the residual images, but no additional nuclear bar candidates were recovered with this technique.

The remaining galaxies could not be fit with 2-D models due to either insufficient signal-to-noise in the galaxy component or irregular/peculiar morphology. For example, Mrk 334 or NGC 4388 are obviously too irregular or dusty to fit with smooth elliptical isophotes. More regular galaxies such as NGC 3362 or UM 146 are sufficiently faint that the galaxy is undetected over much of even the small NIC1 field-of-view. Finally, while Seyferts like NGC 5347 and UGC 12138 are bright, the nuclear PSF dominates the signal from the galaxy out to nearly $1''$ and at larger radii the galaxy is too faint for an acceptable fit. As it is not possible to accurately model the galaxy light distribution for these remaining objects in our sample, we cannot reliably measure the apparent magnitude of the nuclear point source.

5. Discussion

There are now a large number of galaxies with nuclear bars (Buta & Crocker 1993; Friedli 1996; Jungwiert et al. 1997) and no evidence for any preferred position angle of the nuclear bar with respect to the host galaxy bar. The apparently random orientation between the host and nuclear bars is consistent with models that do not predict the nuclear and host galaxy bar to be kinematically coupled (e.g. Friedli 1999).

Of the 24 galaxies in our sample, five (Mrk 266, Mrk 334, Mrk 744, NGC 4388, and NGC 5033) are sufficiently disturbed or high inclination systems in which we would not expect to see a nuclear bar if one were present. In the remaining 19 galaxies, our sensitivity to nuclear bars of a given semimajor axis length is a function of distance, galaxy inclination, and the brightness of the nuclear point source. The *gaseous* nuclear bar in Circinus studied by Maiolino et al. (2000) has a semimajor axis length of approximately 100pc and is one of the shortest known nuclear bars. We would have detected nuclear bars 100pc or longer in 13 of these galaxies and in fact do detect a bar in four, with projected semimajor axes ranging in size from nearly 300 to 900pc (see Table 2). For the remaining six, more distant galaxies, the average minimum projected semimajor axis length we are sensitive to is $\sim$ 160pc. While in many cases the NIC1 field of view is not large enough to be sensitive to nuclear bars that extend to a kiloparsec, ground-based NIR imaging of these galaxies by McLeod & Rieke (1995) and Mulchaey et al. (1997) were sensitive to nuclear bars at these scales.

All four of our nuclear bar candidates meet the bar selection criteria used by Mulchaey et al. (1997) and Knapen et al. (2000) to select host galaxy bars. Mrk 573 and Mrk 270 have dust lanes along one edge of the nuclear bar in the visible–NIR colormaps (see Figure 5) which then turn sharply inwards to the nucleus, forming the straight dust lanes across the nucleus observed by Martini & Pogge (1999). This dust morphology is similar to what is observed in host galaxy bars (Quillen et al. 1995; Regan et al. 1997). If these dust lanes do trace shocks along the leading edge of the nuclear bar, they must extend to their corotation radius to produce such strong shocks (Maciejewski et al. 2001). The dust morphology associated with the nuclear bars in Mrk 471 and NGC 5929 appears more irregular. Mrk 471 does also show evidence for a straight dust lane crossing the nucleus perpendicular to the nuclear bar position angle, similar to what is seen in Mrk 573 and Mrk 270, but there is no evidence for dust along the nuclear bar at larger radii. The circumnuclear region of NGC 5929 is quite irregular. There is some clumpy dust perpendicular to the nuclear bar position angle, but no evidence for coherent structures on larger scales that are associated with the nuclear bar.

Because the nuclear bars discovered in nearby galaxies have small angular sizes, only a small fraction of the ~ 40 known nuclear bars (Friedli 1999) have kinematic data available. Maiolino et al. (2000) obtained kinematic information for the gaseous nuclear bar in Circinus that supported their nuclear bar interpretation, while Emsellem et al. (2001) obtained spectra of four nuclear bars in nearby galaxies and found that three of them were well-fit by a nuclear bar model. These studies suggest that there are true nuclear bars and, from the study of Emsellem et al. (2001), that they can be made up of old stars. Kinematic information for the four nuclear bar candidates in these Seyferts could confirm that they follow the dynamics expected for nuclear bars.

We have found nuclear bar candidates in four of the 24 Seyferts in this sample using a well-defined, quantitative selection technique based on the NIR surface brightness distribution. Our observations were sensitive to nuclear bars with a semimajor axis length as small as ~ 100pc for 13 of these galaxies and to approximately twice this length for six additional galaxies. Previous studies of the frequency of nuclear bars in spirals generally found them in 20 – 30% of galaxies (Buta & Crocker 1993; Friedli 1996; Regan & Mulchaey 1999; Erwin & Sparke 1999b; Márquez et al. 2000), in good agreement with the fraction we report here, although the selection techniques and spatial resolution vary considerably between these different investigations. Our result that nuclear bars are present in only a minority of AGN strongly suggests that they are not responsible for removing angular momentum and transporting fuel from the host galaxy to the nuclear (~ 10 pc) region in most Seyferts. As we have used a well-defined and quantitative method of selecting nuclear bars, the relative frequency of nuclear bars in AGN and non-active galaxies could be studied with a future control sample.

We would like to thank Chien Peng for providing us with a copy of the GALFIT code and both referees for some helpful comments. Witold Maciejewski also provided us with many useful comments that helped to clarify the discussion of the different types of nuclear bars. Support for this work was provided by NASA through grant number GO-07867.01-96A from the Space Telescope Science Institute, which is operated by the Association of Universities for Research in Astronomy, Inc., under NASA contract NAS5-26555. This research has made use of the NASA/IPAC Extragalactic Database (NED) which is operated by the Jet Propulsion Laboratory, California Institute of Technology, under contract with the National Aeronautics and Space Administration.

A. Notes on Individual Objects

For each galaxy we briefly summarize the NIR morphology and discuss the quality of the elliptical isophote and 2-D fits. We also mention any previous observations which may affect our interpretation.

Mrk 334 – This interacting system has a tidal arm visible in both the J and H images. The nuclear point source is particularly bright: both the first Airy ring and a second diffraction ring is visible at $0.7''$ in the H image. The presence of the PSF features results in limited sensitivity to any potential nuclear bar with semimajor axis < 310 pc. Because this is an interacting system, a nuclear bar is probably not required to remove angular momentum from gas in the host galaxy to transport it inwards.

Mrk 471 – The nuclear bar candidate in this galaxy is apparent in grayscale images, as is the break in the ellipticity and position angle at $\sim 1.3''$, which corresponds to a projected ~ 860 pc semimajor axis length. This projected semimajor axis length is comparable to some host galaxy bars (e.g. NGC 1068), yet this galaxy also has a clear host galaxy bar, which is apparent on larger scales in the grayscale. The straight dust lanes noticed by Martini & Pogge (1999) are nearly perpendicular to the position angle of the nuclear bar within the bar semiminor axis, although they do not appear to trace the edge of the bar at larger radii, as seen in Mrk 270.

Mrk 744 – Keel (1980) first noticed that Seyfert 1s are found much less frequently in edge-on systems compared Seyfert 2s. Dust obscuration from the host galaxy was suggested to be particularly important in this high-inclination system by Goodrich & Osterbrock (1983) and the bright, NIR nuclear point source is further evidence that it only appears as a weak broad-line system due to host galaxy dust. The elliptical isophotes only poorly fit the morphology of this inclined and interacting system.

UGC 12138 – Interpretation of the circumnuclear structure in this galaxy is complicated by the strong nuclear point source. As in Mrk 334, the first Airy ring and a second ring at $0.7''$ are visible in the H surface brightness profile. These features limit the sensitivity to a nuclear bar with semimajor axis < 350 pc. At larger radii, the ellipticity starts to increase again at the position angle of the host galaxy bar.

NGC 5033 – This nearly edge-on galaxy hosts a Seyfert 1.9 nucleus and is conspicuously brighter in the NIR than at visible wavelengths, suggesting that host galaxy dust contributes to the obscuration of the nuclear region. The position angle of ~ 160 degrees measured in the (poor) elliptical isophote fits is in good agreement with the value measured by Thean et al. (1997).

NGC 5252 – The nuclear point source in this Seyfert 1.9 is relatively weak and only slightly affects the ellipticity distribution for $< 0.2''$. This galaxy is well-fit by a Nuker profile.

NGC 5273 – There is a "spike" in the ellipticity distribution at $r_J \sim 0.5''$ or $r_H \sim 0.6''$ (corresponding to a projected semimajor axis length of ~ 40 pc). While this spike is of sufficient amplitude to meet our nuclear bar selection criteria, the fact that the variation in ellipticity occurs at a larger semimajor axis in the longer wavelength filter suggests that this is probably an artifact of the strong nuclear point source. Dust may also be a factor as the ellipticity variation is greater at J than at H. For these reasons we do not classify this spike as a nuclear bar candidate.

NGC 5674 – While there is a large ellipticity variation at J, it is not present at H. There is a significant amount of amorphous dust perpendicular to the position angle of this ellipticity, thus the ellipticity change is very likely due to dust. The nuclear point source is also bright in this galaxy and it clearly compromises the elliptical isophote fits to the inner region. We therefore do not consider this to be a nuclear bar candidate. The underlying galaxy was otherwise sufficiently bright and regular for GALFIT to model the surface brightness distribution.

UM 146 – There is a clear jump in the H surface brightness profile due to the first Airy ring of the nuclear PSF. The galaxy appears otherwise quite faint and compact; the elliptical isophotes only extend to $\sim 2''$.

Mrk 461 – This galaxy has a relatively smooth surface brightness profile, but there was not sufficient signal-to-noise over a large enough range in radius to fit the underlying galaxy profile shape.

Mrk 266 – Mrk 266SW is in the midst of a merger and exhibits a very chaotic appearance which precludes a reliable elliptical isophote fit. The NIR peak shown in Figure 2 is actu-

ally offset from the peak in the visible-wavelength F606W image. The extremely irregular morphology and red nucleus of this galaxy strongly suggests that host galaxy material is obscuring the line of sight to the active nucleus.

Mrk 270 – There is a good nuclear bar candidate visible in the J and H images that corresponds to the drop in the ellipticity at $\sim 1.9''$, corresponding to a projected physical semimajor axis length of ~ 350 pc. There are two dust lanes in the nuclear region that trace the edges of the nuclear bar and then turn abruptly to cross the nucleus as a straight dust lane. Outside $2''$ the position angle changes to match that of the host galaxy bar.

Mrk 573 – This is the best example of a double-barred galaxy in the sample. The nuclear bar candidate previously noticed by Pogge & DeRobertis (1993) and Capetti et al. (1996) is readily apparent in the NIR surface brightness. The dust lane morphology is similar to Mrk 471, where the dust lanes trace the edge of the nuclear bar and then turn abruptly to cross the nucleus perpendicular to the bar position angle as a straight dust lane.

NGC 1068 – The elliptical isophote fits to this galaxy were compromised by significant circumnuclear dust and the bright nuclear point source. The nuclear point source is particularly prominent at H, which supports the interpretation that this galaxy harbors a dust-obscured broad line region, first suggested by the polarization study by Miller & Antonucci (1983). While this nearly face-on galaxy shows significant radial ellipticity variations in J and H, these variations are clearly uncorrelated as they reach a peak at $\sim 1.5''$ in J, but $\sim 0.7''$ in H. The much larger variation in J is likely due to dust. The ellipticity variation at $0.7''$ in H is coincident with a variation in the surface brightness profile and is due to the PSF diffraction pattern.

NGC 1144 – This interacting system has relatively smooth NIR surface brightness distribution in its central few arcseconds, although the dust lane visible in the J and H grayscale images illustrates the more disturbed morphology at larger scales.

NGC 3362 – Elliptical isophotes are a relatively poor fit to this galaxy outside of $\sim 1''$ as the galaxy is extremely faint.

NGC 3982 – McLeod & Rieke (1995) did not find evidence of the host galaxy bar in their K image of this "SAB" galaxy. While our ellipse fits and GALFIT model do recover a larger ellipticity than that suggested by the axis ratio of $b/a \sim 0.9$ they measured, our images are not sufficiently sensitive on the large scales necessary to detect a host galaxy bar.

NGC 4388 – This edge-on galaxy has an extremely chaotic appearance at small scales, at least partially due to a host galaxy dust lane passing to the immediate north of the nucleus and significantly attenuating even the $H-$band light. This galaxy cannot be well fit with

elliptical isophotes.

NGC 5347 – Regan & Mulchaey (1999) noticed a straight dust lane crossing the nucleus in this galaxy and suggested that it contains a nuclear bar, although Martini & Pogge (1999) did not find this structure in their color maps. There is a slight jump in the ellipticity at $\sim 0.5''$, corresponding to a projected semimajor axis length of ~ 80 pc, but the strength of the ellipticity variation is much greater at J than at H, suggesting that dust is responsible. Dust is clearly present to the immediate south of the nucleus in Figure 2 of Martini & Pogge (1999), nearly perpendicular to the position angle of the nuclear bar and this dust is likely responsible for the distortion in the surface brightness distribution. This dust also corresponds to the curved dust lane observed by Regan & Mulchaey (1999) on which they base their identification of a *gaseous* nuclear bar.

NGC 5695 – This Seyfert 2 is quite bright and well fit by a Nuker profile. The nuclear point source is sufficiently faint that GALFIT did not need to include a nuclear point source in the 2-D model. At large radii the ellipticity starts to increase at the position angle of the host galaxy bar.

NGC 5929 – The nuclear bar candidate in this interacting system has a semimajor axis of $\sim 1.7''$, corresponding to a projected semimajor axis length of ~ 280 pc. The ellipticity variation is stronger in the J elliptical isophote fits than at H and there is dust nearly perpendicular to the nuclear bar candidate in the Martini & Pogge (1999) color map. The inner region of this galaxy is sufficiently regular to be well-fit by GALFIT and the fit residuals show the signature of the nuclear bar.

NGC 7674 – Polarized, broad emission lines were first detected in this object by Miller & Goodrich (1990). The extremely bright nuclear point source compared to the other Seyfert 2s (with the exception of NGC 1068) reinforce its interpretation as an obscured Seyfert 1. The elliptical isophotes are a reasonable match to the surface brightness distribution of this galaxy outside the immediate influence of the nuclear source.

NGC 7682 – This Seyfert 2 was not well fit by a Nuker profile and instead was fit with a Sérsic profile. The nuclear point source is sufficiently faint that GALFIT did not need to include it in the 2-D fit to the surface brightness distribution.

REFERENCES

Athanassoula, E. 1992, MNRAS, 259, 345

Buta, R. 1986a, ApJS, 61, 609

Buta, R. 1986b, ApJS, 61, 631

Buta, R. & Crocker, D.A. 1993, AJ, 105, 1344

Capetti, A., Axon, D.J., Macchetto, F., Sparks, W.B., & Boksenberg, A. 1996, ApJ, 469, 554

Carollo, C.M., Stiavelli, M., & Mack, J. 1998, AJ, 116, 68

Carollo, C.M., & Stiavelli, M. 1998, AJ, 115, 2306

Colina, L., & Wada, K. 2000, ApJ, 529, 845

De Robertis, M.M., Yee, H.K.C., & Hayhoe, K. 1998, ApJ, 496, 93

de Vaucouleurs, G. 1975, ApJS, 29, 193

Elias, J.H., Frogel, J.A., Matthews, K., & Neugebauer, G. 1982, AJ, 87, 1029

Elmegreen, B.G., Elmegreen, D.M., Brinks E., Yuan, C., Kaufman, M., Klarić, M., Montenegro, L., Struck, C., & Thomasson, M. 1998, ApJ, 503, L119

Emsellem, E., Greusard, D., Combes, F., Friedli, D., Leon, S., Pécontal, E., Wozniak, H. 2001, A&A, 368, 52

Erwin, P. & Sparke, L.S. 1999a, ApJ, 521, L37

Erwin, P. & Sparke, L.S. 1999b, in ASP Conf. Ser. 182, Galaxy Dynamics, ed. D.R. Merritt & J.A. Sellwood (San Fransciso: ASP)

Faber, S.M. et al. 1997, AJ, 114, 1771

Friedli, D. & Martinet, L. 1993, A&A, 277, 27

Frieldi, D. 1996, in Buta, R. et al., eds. ASP Conf. Ser. Vol. 91, Proc. IAU Colloq. 157, Barred Galaxies. Astron. Soc. Pac., San Fransisco, p. 378

Frieldi, D. 1999, in Beckman, J.E. & Mahoney, T.J., eds. ASP Conf. Ser. Vol. 187, The Evolution of Galaxies on Cosmological Timescales. Astron. Soc. Pac., San Fransisco, p. 88

Fuentes-Williams, T. & Stocke, J.T. 1988, AJ, 96, 1235

Goodrich, R. W., & Osterbrock, D. E. 1983, ApJ, 269, 416

Ho, L.C., Filippenko, A.V., & Sargent, L.W. 1997a, ApJ, 487, 591

Ho, L.C., Filippenko, A.V., & Sargent, L.W. 1997b, ApJS, 112, 315

Ho, L.C., Filippenko, A.V., Sargent, L.W., & Peng, C.Y. 1997c, ApJS, 112, 391

Ho, L.C. 1999, ApJ, 516, 672

Huchra, J. & Burg, R. 1992, ApJ, 393, 90

Jedrzejewski, R.I. 1987, MNRAS, 226, 747

Jungwiert, B., Combes, F., Axon, D.J. 1997, A&AS, 125, 479

Keel, W.C. 1980, AJ, 85, 198

Knapen, J.H., Shlosman, I., Peletier, R.F., ApJ, 529, 93

Kormendy, J. 1979, ApJ, 227, 714

Krist, J.E. & Hook, R.N. 1997, "NICMOS PSF variations and Tiny Tim simulations," Proceedings of the 1997 HST Calibration Workshop, p. 192

Krist, J.E. & Hook, R.N. 1999, The Tiny Tim User's Guide (Baltimore: STScI)

Laine, S., Knapen, J.H., Pérez-Ramírez, D., Doyon, R., & Nadeau, D. 1999, MNRAS, 302, L33

Lauer, T.R., et al. 1995, AJ, 110, 2622

Lauer, T.R., Faber, S.M., Ajhar, E.A., Grillmair, C.J., & Scowen, P.A. 1998, AJ, 116, 2263

Maciejewski, W. & Sparke, L.S. 1997, ApJ, 484, L117

Maciejewski, W. & Sparke, L.S. 2000, MNRAS, 313, 745

Maciejewski, W., Teuben, P.J., Sparke, L.S., & Stone, J.M. 2001, MNRAS, *submitted*

Maiolino, R., Alonso-Herrero, A., Anders, S., Quillen, A., Rieke, M.J., Rieke, G.H., & Tacconi-Garman, L.E. 2000, ApJ, 531, 219

Malkan, M.A., Gorjian, V., & Tam, R. 1998, ApJS, 117, 25

Martini, P. & Pogge, R.W. 1999, AJ, 118, 2646

Márquez, I. et al. 1999, A&AS, 140, 1

Márquez, I. et al. 2000, A&A, 360, 431

McLeod, K.K. & Rieke, G.H. 1995, ApJ, 441, 96

Miller, J.S. & Goodrich, R.W. 1983, ApJ, 271, L7

Miller, J.S. & Goodrich, R.W. 1990 ApJ, 355, 456

Montenegro, L.E., Yuan, C., & Elmegreen, B.G. 1999, ApJ, 520, 582

Mulchaey, J.S. & Regan, M.W. 1997, ApJ, 482, 135

Mulchaey, J.S., Regan, M.W., & Kundu, A. 1997, ApJS, 11, 299

Nelson, C.H., MacKenty, J.W., Simkin, S.M., Griffiths, R.E. 1996, ApJ, 466, 713

Osterbrock, D.E. & Martel, A. 1993, ApJ, 414, 552

Peng, C.Y., Ho., L.C., & Impey, C. 2001, *in preparation*

Persson, S.E., Murphy, D.C., Krzeminski, W., Roth, M., & Rieke, M.J. 1998, AJ, 116, 2475

Pfenniger, D. & Norman, C. 1990, ApJ, 363, 391

Phillips, A.C., Illingworth, G.D., MacKenty, J.W., & Franx, M. 1996, AJ, 111, 1566

Pogge, R.W. & DeRobertis, M.M. 1993, ApJ, 404, 563

Quillen, A.C., Frogel, J.A., Kenney, J.D.P., Pogge, R.W., Depoy, D.L. 1995, ApJ, 441, 549

Quillen, A.C., Alonso-Herrero, A., Rieke, M. J., McDonald, C., Falcke, H., & Rieke, G. H. 1999, ApJ, 525, 685

Quillen, A.C., McDonald, C., Alonso-Herrero, A., Lee, A., Shaked, S., Rieke, M.J., & Rieke, G.H. 2001, ApJ, 547, 129

Ravindranath, S., Ho, L.C., Peng, C.Y., Filippenko, A.V., & Sargent, W.L.W. 2001, AJ, *in press*

Regan, M.W., Vogel, S.N, & Teuben, P.J. 1997, ApJ, 482, L143

Regan, M.W. & Mulchaey, J.S. 1999, AJ, 117, 2676

Rest, A., van den Bosch, F.C., Jaffe, W., Tran, H., Tsvetanov, Z., Ford, H.C., Davies, J., & Schafer, J. 2001, AJ, in press

Sérsic, J.L. 1968, Atlas de Galaxias Australes (Córdoba: Obs. Astron., Univ. Nac. Córdoba)

Shlosman, I., Frank, J., & Begelman, M.C. 1989, Nature, 338, 45

Stephens, A.W., Frogel, J.A., Ortolani, S., Davies, R., Jablonka, P., Renzini, A., & Rich, R.M. 2000, AJ, 119, 419

Stover, R.J. 1988,

Thompson, R.I. & Corbin, M. 1999, Ap&SS, 266, 79

Thean, A.H.C., Mundell, C.G., Pedlar, A., & Nicholson, R.A. 1997, MNRAS, 290, 15

Tonry, J.L., Dressler, A., Blakeslee, J.P., Ajhar, E.A., Fletcher, A.B., Luppino, G.A., Metzger, M.R., Moore, C.B. 2001, ApJ, 546, 641

Tully, R.B. 1988, Nearby Galaxies Catalog (Cambridge: Cambridge Univ. Press)

van Dokkum, P.G., & Franx, M. 1995, AJ, 110, 2027

Yahil, A., Tammann, G.A., & Sandage, A. 1977, ApJ, 217, 903

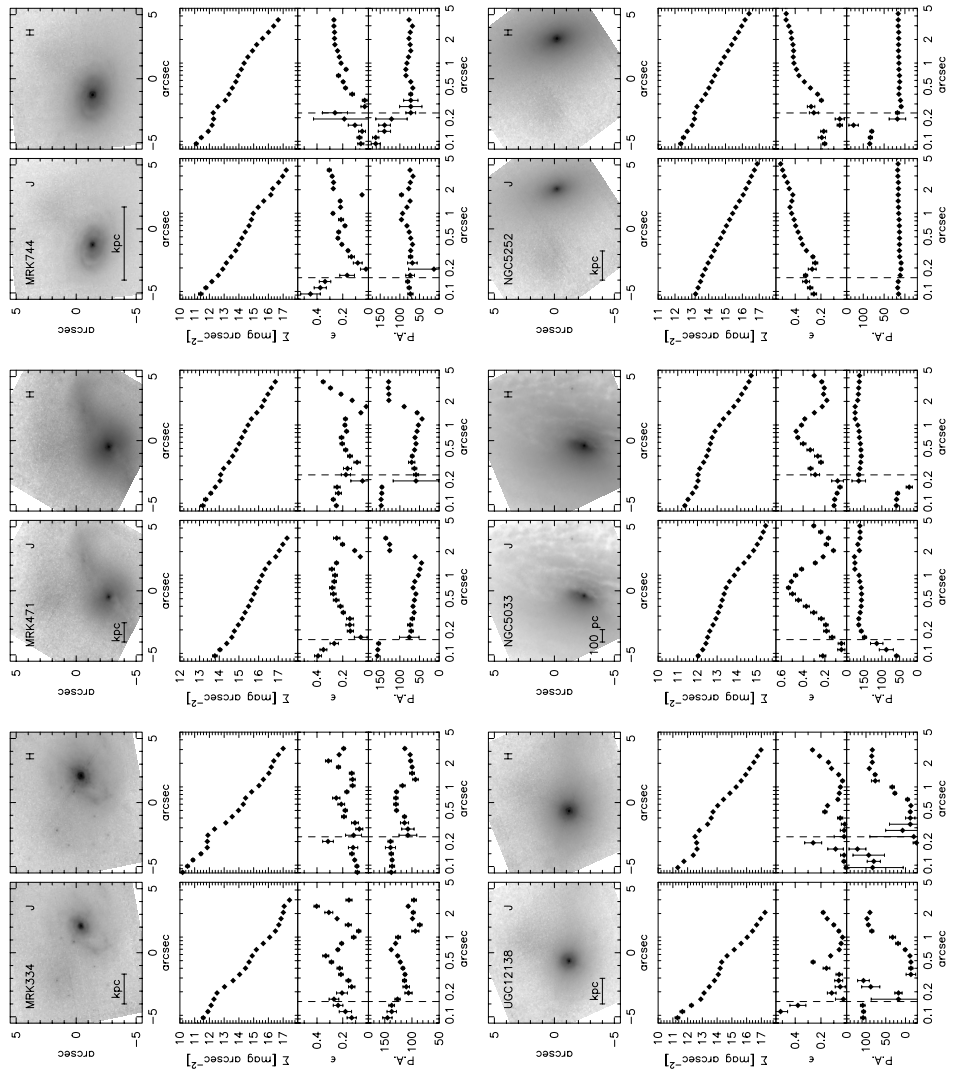

Fig. 1.— Grayscale images and surface brightness, ellipticity, and position angle profiles as a function of semimajor axis for Mrk 334, Mrk 471, Mrk 744, UGC 12138, NGC 5033, and NGC 5252. The left panels in each plot correspond to the J image of the galaxy and the right panels to the H image. The grayscale images (*top panels*) are on a log scale and have been rotated so that north is up and east is to the left. The remaining panels show the surface brightness profile, ellipticity, and position angle (measured north through east) as a function of the ellipse semimajor axis. The dashed, vertical lines mark the location of first Airy ring, and designate the smallest angular scale at which we could detect nuclear bars (see Section 3).

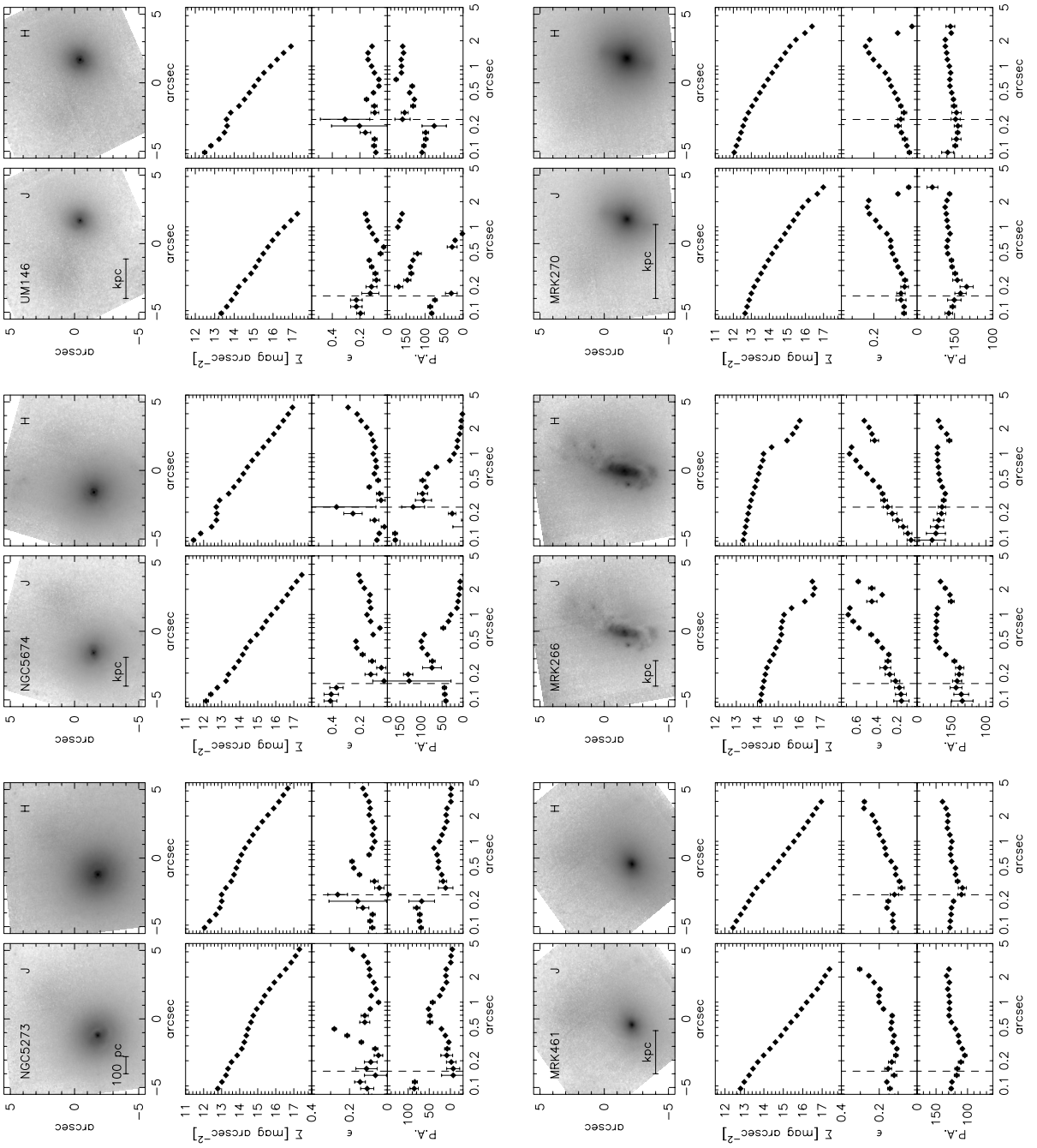

Fig. 2.— Same as Figure 1 for NGC 5273, NGC 5674, UM 146, Mrk 461, Mrk 266SW, and Mrk 270.

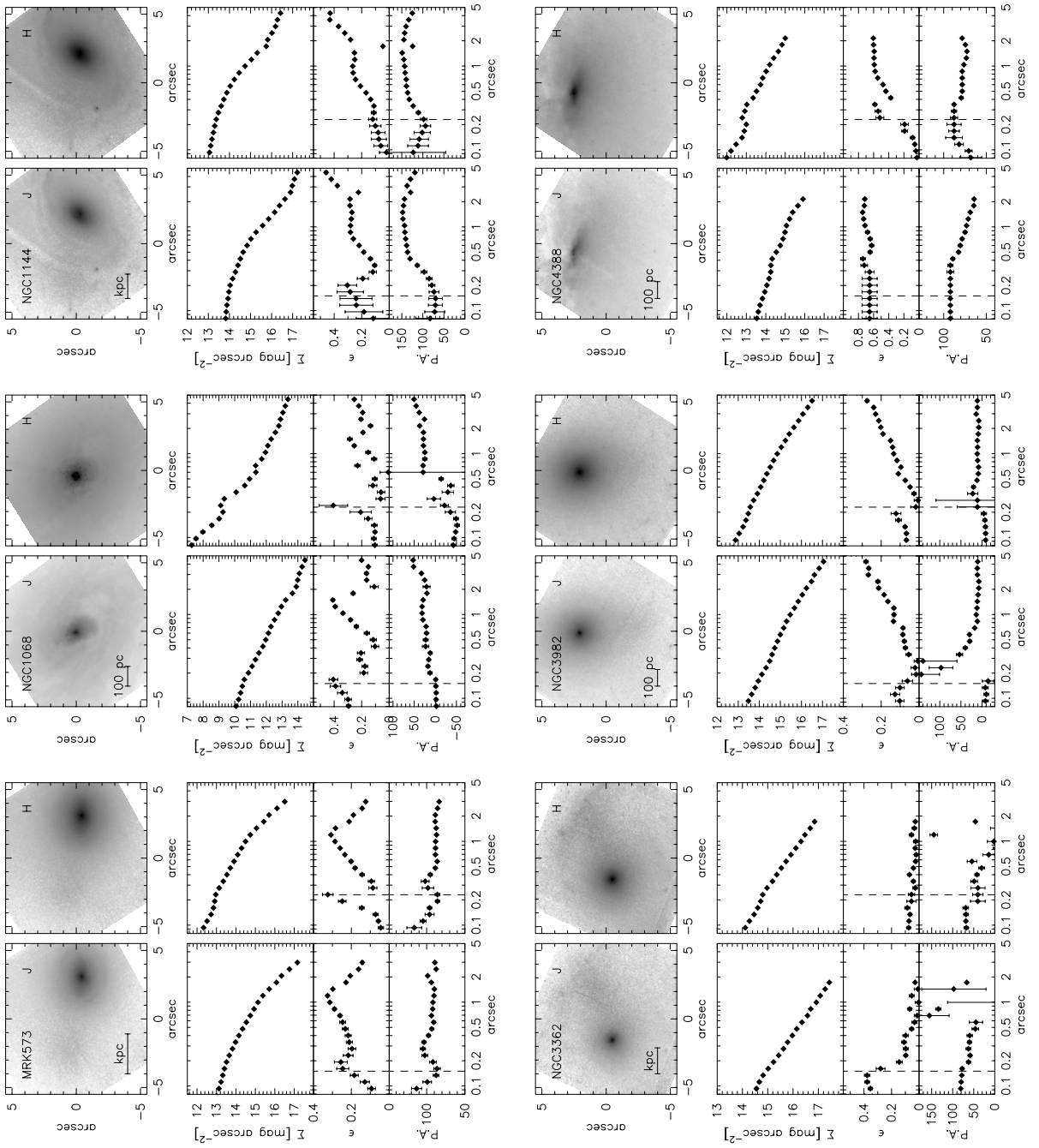

Fig. 3.— Same as Figure 1 for Mrk 573, NGC 1068, NGC 1144, NGC 3362, NGC 3982, and NGC 4388.

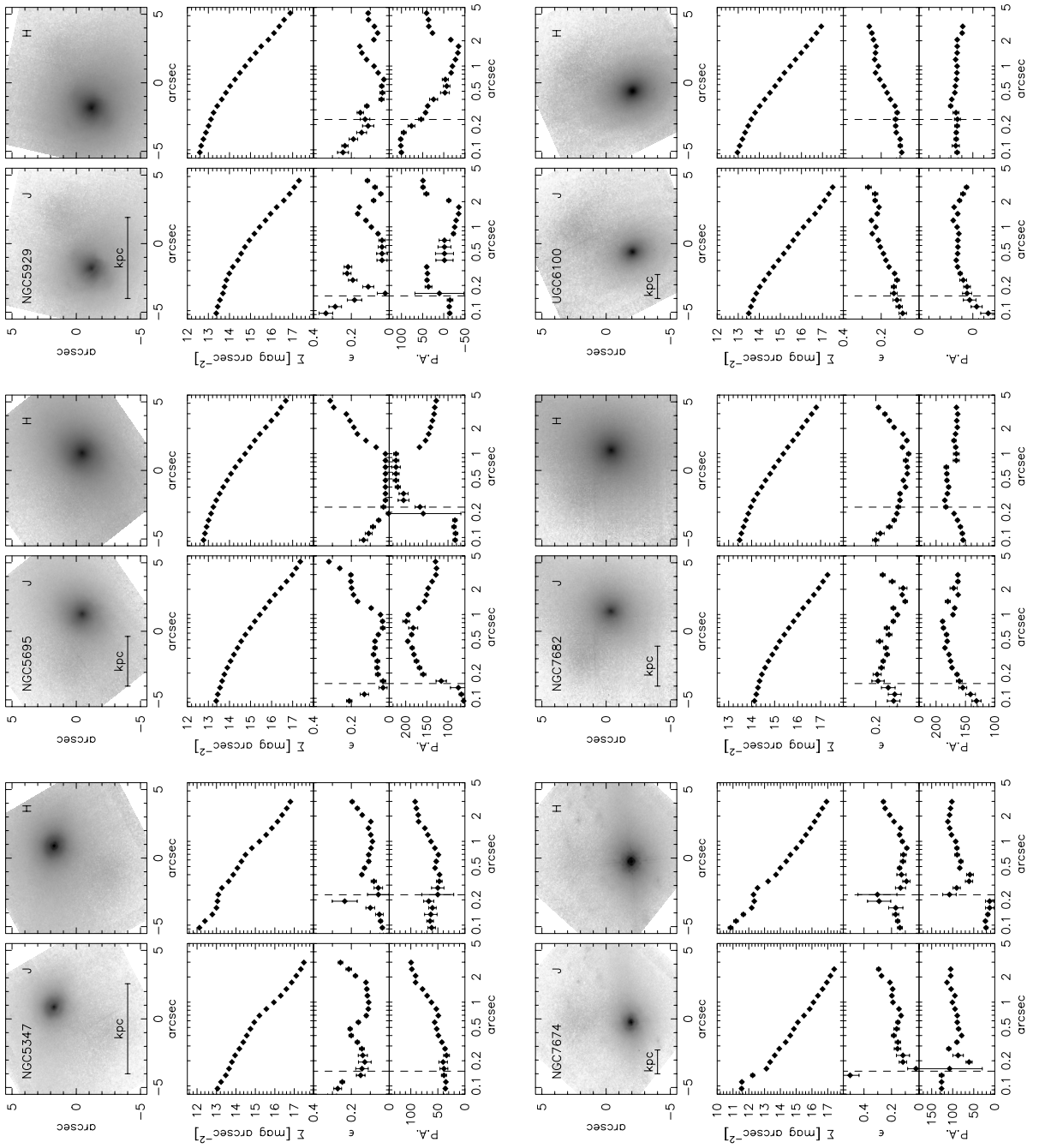

Fig. 4.— Same as Figure 1 for NGC 5347, NGC 5695, NGC 5929, NGC 7674, NGC 7682, and UGC 6100.

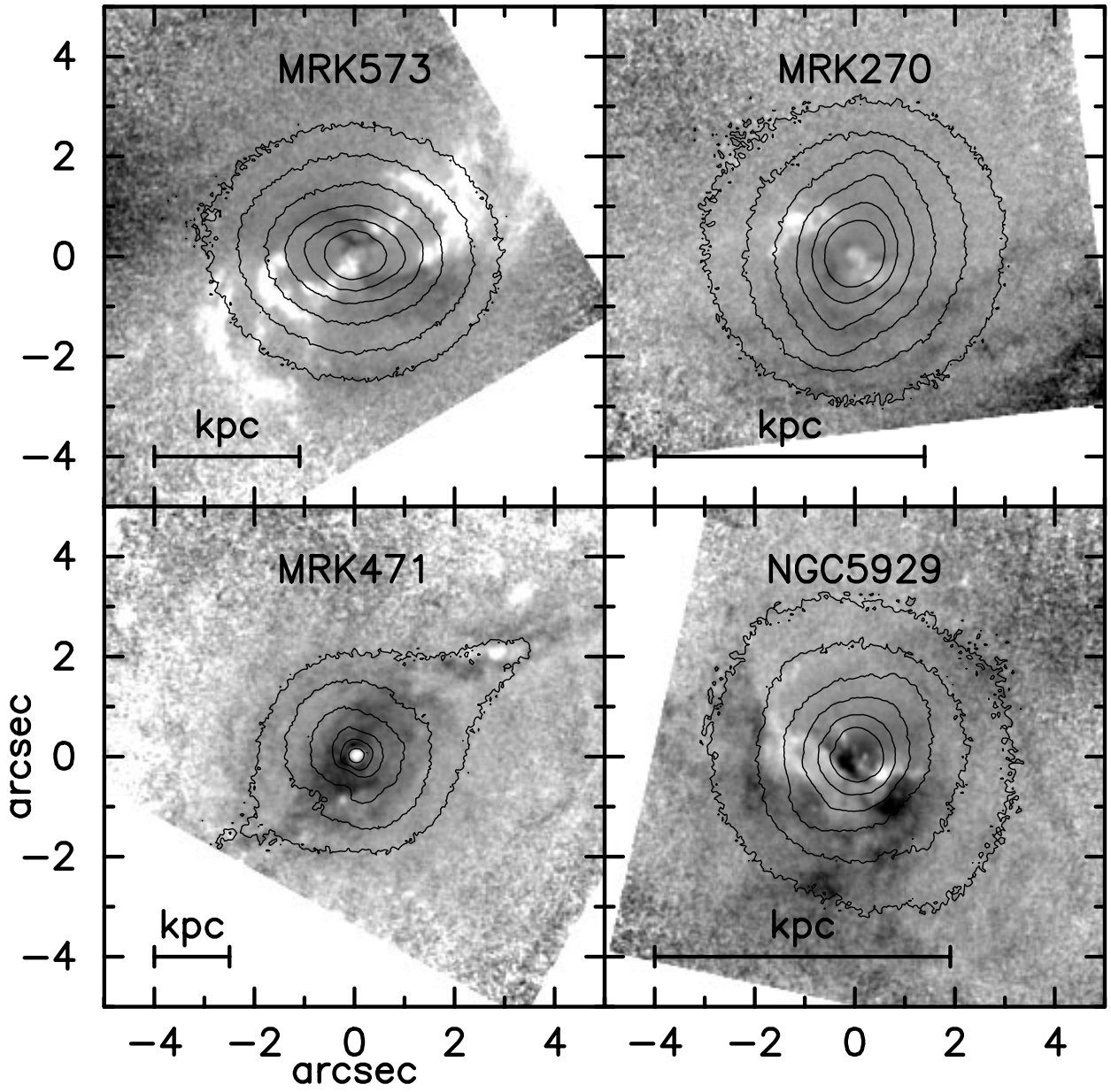

Fig. 5.— $V-H$ colormaps and $H-$band surface brightness contours of the four nuclear bar candidates. In Mrk 573 the two spiral dust lanes (dark on this greyscale) appear to trace the leading edge of the nuclear bar. At larger radii these two dust lanes are lit up by the nuclear source and form the ionization cone. They turn blue on this colormap due to the presence of bright Hα emission in the F606W filter bandpass. Mrk 270 and Mrk 471 show weaker evidence for an association between the dust morphology and the nuclear bar, while the dust morphology in NGC 5929 exhibits no obvious, coherent structure.

Table 1. Sample Characteristics

Name	Other ID	Seyfert Type	Galaxy Type	Note	Distance	pc/″
Mrk 334		1.8	Pec	Disturbed	88.4	429
Mrk 471		1.8	SBa		137.3	666
Mrk 744	NGC 3786	1.8	SAB(rs)a pec	Interacting	36.1	175
UGC 12138	2237+07	1.8	SBa		102.8	498
NGC 5033		1.9[a]	SA(s)c	Edge On	21.3	103
NGC 5252		1.9	SO		90.7	440
NGC 5273		1.9[a]	SA(s)0^0		16.5	80
NGC 5674		1.9	SABc		98.1	476
UM 146	0152+06	1.9	SA(rs)b		71.6	347
Mrk 461		2	S		65.6	318
Mrk 266	NGC5256	2	Comp Pec		111.0	538
Mrk 270	NGC5283	2	SO?		38.2	185
Mrk 573		2	(R)SAB(rs)O+:		71.0	344
NGC 1068		2	SAb		14.4	70
NGC 1144		2	RingB	Interacting	116.4	564
NGC 3362		2	SABc		108.7	527
NGC 3982		2	SAB(r)b:		17.0	82
NGC 4388		2	SA(s)b: sp	Edge On	16.8	81
NGC 5347		2	(R')SB(rs)ab		31.4	152
NGC 5695	Mrk 686	2	SBb		56.9	276
NGC 5929		2	Sab: pec	Interacting	34.9	169
NGC 7674	Mrk 533	2	SA(r)bc pec		118.5	575
NGC 7682		2	SB(r)ab		70.8	343
UGC 6100	A1058+45	2	Sa?		117.6	570

[a]Classified as type 1.5 by Ho et al. (1997b)

Note. — Properties of the galaxies observed with the NICMOS Camera 1 for program GO7867, along with NGC 1068. Columns 1 & 2 list the most common names for the targets, and column 3 lists its Seyfert type as reported by Osterbrock & Martel (1993). In column 4 we have compiled the morphological type for the host galaxy from NED, while in column 5 we have provided additional comments on the galaxy morphology. Column 6 lists the distance of the galaxy in Mpc (from Tully 1988; Ho et al. 1997c; Tonry et al. 2001, or using Yahil et al. (1977), assuming $H_0 = 75$ km s^{-1} Mpc^{-1}). Column 7 contains the projected size in parsecs of one arcsecond at the distance of the galaxy.

Table 2. Properties of the Nuclear Bar Candidates

Name	PA [degree]	a [arcsec]	a_p [parsec]	Host bar PA
Mrk 573	90	1.2	410	0
Mrk 270	160	1.9	350	
NGC 5929	150	1.7	280	
Mrk 471	60	1.3	860	130

Note. — Properties of the nuclear bars in our sample. Column 2 lists the position angle (north through east) of the nuclear bar candidates for each of the galaxies in column 1. Columns 3 and 4 provide the semimajor axis length of the bar in arcseconds and the corresponding projected size in parsecs. Column 5 gives the position angle of the host galaxy bar, if present.

Table 3. Galaxy Profile Fits

Name	m_H^{nuc} [mag]	μ_b [mag/arcsec^2]	r_b (r_s) [$''$]	α (n)	β	γ	Function
Mrk 270	15.8		0.61	1.74			Sérsic
Mrk 573	15.9	13.9	0.61	2.95	1.54	0.70	Nuker
NGC 3982	16.6	14.5	0.73	4.96	1.08	0.71	Nuker
NGC 5252	15.8	15.6	2.12	0.28	1.71	0.52	Nuker
NGC 5273	14.9	14.2	0.80	9.18	1.37	0.60	Nuker
NGC 5674	13.9	13.9	0.45	4.41	1.50	0.46	Nuker
NGC 5695		13.8	0.45	3.55	1.38	0.66	Nuker
NGC 5929	17.1	13.3	0.29	1.96	1.40	0.46	Nuker
NGC 7674	13.4	16.7	2.60	0.18	2.23	0.45	Nuker
NGC 7682			0.41	1.94			Sérsic
UGC 6100		12.7	0.11	1.88	1.45	0.49	Nuker

Note. — Galaxy profile fits to the F160W images. For each galaxy in column 1 we list the H magnitude of the nuclear PSF in column 2 and the best fitting parameters of a Nuker (Sérsic) profile in columns 3 – 7. Column 8 identifies which function was fit to each galaxy. These fitting functions are defined in section 4.